



저작자표시-비영리-변경금지 2.0 대한민국

이용자는 아래의 조건을 따르는 경우에 한하여 자유롭게

- 이 저작물을 복제, 배포, 전송, 전시, 공연 및 방송할 수 있습니다.

다음과 같은 조건을 따라야 합니다:



저작자표시. 귀하는 원저작자를 표시하여야 합니다.



비영리. 귀하는 이 저작물을 영리 목적으로 이용할 수 없습니다.



변경금지. 귀하는 이 저작물을 개작, 변형 또는 가공할 수 없습니다.

- 귀하는, 이 저작물의 재이용이나 배포의 경우, 이 저작물에 적용된 이용허락조건을 명확하게 나타내어야 합니다.
- 저작권자로부터 별도의 허가를 받으면 이러한 조건들은 적용되지 않습니다.

저작권법에 따른 이용자의 권리는 위의 내용에 의하여 영향을 받지 않습니다.

이것은 [이용허락규약\(Legal Code\)](#)을 이해하기 쉽게 요약한 것입니다.

[Disclaimer](#)

공학석사 학위논문

Synthesis of fluorescent naphthalimide-
functionalized Fe₃O₄ nanoparticles and their
application for the selective detection of Zn²⁺
present in contaminated soil

나프탈이미드 기반 형광 산화철나노입자의
합성과 오염토에 존재하는 아연 이온의 선택적
검출

2017년 2월

서울대학교 대학원

건설환경 공학부

김 경 태

Synthesis of fluorescent naphthalimide-
functionalized Fe₃O₄ nanoparticles and
their application for the selective detection
of Zn²⁺ present in contaminated soil


나프탈이미드 기반 형광 산화철나노입자의 합성과
오염토에 존재하는 아연 이온의 선택적 검출

지도 교수 박 준 범

이 논문을 공학석사 학위논문으로 제출함
2017년 2월

서울대학교 대학원
건설환경공학부
김 경 태

김경태 석사 학위논문을 인준함
2017년 2월

위 원 장 정 충 기 (인) 

부위원장 박 준 범 (인) 

위 원 최 용 주 (인) 

Abstract

Synthesis of fluorescent naphthalimide-functionalized Fe₃O₄ nanoparticles and their application for the selective detection of Zn²⁺ present in contaminated soil

Kim, Kyung Tae

Department of Civil and Environmental Engineering

The Graduate School

Seoul National University

A fluorescent dopamine–naphthalimide–dipicolylamine (DPA) was synthesized as a sensing receptor for Zn²⁺. Naphthalimide-DPA (**2**) was immobilized onto the surface of iron oxide nanoparticle to prepare a hybrid nanomagnet **1-Fe₃O₄** for the purpose of selective detection of Zn²⁺ in soil. Naphthalimide–DPA (**2**) and **1-Fe₃O₄** were observed to bind with Zn²⁺, leading to significant increase in fluorescence intensity at 527 nm. The fluorescence increases of **2** (10 μM) and **1-Fe₃O₄** (0.33 wt%) by addition of Zn²⁺ were linear over the [Zn²⁺] range of 0–7 μM and 0–20 μM, respectively. These fluorescence changes were highly selective for Zn²⁺, which were readily monitored even in the presence of other competitive cations. In particular, **1-Fe₃O₄** exhibited an excellent limit of detection determined to be 0.0345 ppb. Furthermore, this system was found to be suitable for detecting Zn²⁺ in a wide pH range of 3–11 and could be reused with the addition of ethylenediaminetetraacetic acid (EDTA). Moreover, nanomagnet **1-Fe₃O₄** was employed for the selective detection and removal of Zn²⁺ from a soil

sample. These results confirm that the use of **1-Fe₃O₄** is a novel and simple method for detecting Zn²⁺ in environmental samples.

Keywords: Zinc, Naphthalimide, Fe₃O₄ nanoparticles, Nanomagnet, Soil Contamination

Student Number: 2015-21280

Contents

Chapter 1 Introduction	1
1.1 General.....	1
1.2 Outline.....	4
Chapter 2 Background.....	5
2.1 Background of the Fluorescence Chemosensor	5
2.1.1 Fluorecence	5
2.1.2 Photo-induced Electron Transfer	6
2.1.3 Chelation Enhanced Fluorescence	8
Chapter 3 Experimental Program.....	9
3.1 Materials and instruments	9
3.2 Spectroscopic methods.....	9
3.3 Detemination of limit of detection for 1-Fe₃O₄	10
3.4 Synthesis	11
3.4.1 Synthesis of iron-oleate complex.....	11
3.4.2 Synthesis of iron oxide nanocrystals.....	11
3.4.3 Synthesis of 1-Fe₃O₄	11
3.4.4 Synthesis of 1-5	13
3.4.5 Synthesis of 1	13
3.4.6 Synthesis of 2	16
3.4.7 Synthesis of 3	18
3.4.8 Synthesis of 4	21
3.5 Soil sampling, spiking, and extraction.....	24

Chapter 4 Experimental Results and Analysis	25
4.1 Synthesis and characterization of nanomagnet 1-Fe₃O₄	25
4.2 Spectroscopic analysis of the response of 2 to Zn ²⁺	29
4.2.1 Selectivity of 2 to Zn ²⁺	29
4.2.2 Zn ²⁺ titration test of 2	34
4.2.3 pH titration test of 2	37
4.2.4 Reversibility test of 2	38
4.3 Spectroscopic analysis of the response of 1-Fe₃O₄ to Zn ²⁺	39
4.3.1 Selectivity of 1-Fe₃O₄ to Zn ²⁺	39
4.3.2 Response time of 1-Fe₃O₄ to Zn ²⁺	42
4.3.3 Zn ²⁺ titration test of 1-Fe₃O₄	43
4.3.4 Reversibility test of 2	45
4.4 Detection of Zn ²⁺ in soil samples	46
 Chapter 5 Conclusions	 48
 Bibliography	 49

List of Figures

Figure 2.1 Mechanism of fluorescence	5
Figure 2.2 Mechanism photo-induced electron transfer.....	7
Figure 2.3 Mechanism of Chelation enhanced fluorescence.....	8
Figure 3.1 ¹ H NMR spectrum of 1 in CD ₃ OD	14
Figure 3.2 ¹³ C NMR spectrum of 1 in CD ₃ OD	15
Figure 3.3 ESI-MS spectrum of 1	15
Figure 3.4 ¹ H NMR spectrum of 2 in CD ₃ OD	16
Figure 3.5 ¹³ C NMR spectrum of 2 in CD ₃ OD	17
Figure 3.6 ESI-MS spectrum of 2	17
Figure 3.7 ¹ H NMR spectrum of 3 in CDCl ₃	19
Figure 3.8 ¹³ C NMR spectrum of 3 in CDCl ₃	19
Figure 3.9 ESI-MS spectrum of 3	20
Figure 3.10 ¹ H NMR spectrum of 4 in CDCl ₃	22
Figure 3.11 ¹³ C NMR spectrum of 4 in CDCl ₃	22
Figure 3.12 ESI-MS spectrum of 4	23
Figure 4.1 Synthesis of nanomagnet 1-Fe₃O₄	26
Figure 4.2 IR spectra of 1 , Fe ₃ O ₄ , and 1-Fe₃O₄	27
Figure 4.3 TEM image of 1-Fe₃O₄ particles	27
Figure 4.4 TGA curve of 1-Fe₃O₄	28
Figure 4.5 Fluorescence spectra of 2 (10 μM) in the presence of various metal ions.....	31
Figure 4.6 Visible emission observed for samples of 2 , 2 /Zn ²⁺ , and 2 /Cd ²⁺ ...	31
Figure 4.7 Fluorescence changes of 2 toward Zn ²⁺ in the presence of various metal ions.....	32
Figure 4.8 Fluorescence spectra of 2 complexed with Zn ²⁺ with the addition of various metal ions	33
Figure 4.9 Zn ²⁺ titration test of 2	35

Figure 4.10 Job's plot for the complexation of 2 with Zn^{2+}	36
Figure 4.11 Benesi–Hildebrand plot	36
Figure 4.12 Fluorescence changes of 2 in solutions with different pH	37
Figure 4.13 Reversibility test result of 2	38
Figure 4.14 Fluorescence spectra of 1-Fe₃O₄ in the presence of various metal ions.....	40
Figure 4.15 Fluorescence spectra of 1-Fe₃O₄ complexed with Zn^{2+} with the addition of metal cations.....	41
Figure 4.16 Time-dependent fluorescence spectra of 1-Fe₃O₄	42
Figure 4.17 Zn^{2+} titration of 1-Fe₃O₄	43
Figure 4.18 Detection limit of 1-Fe₃O₄	44
Figure 4.19 Reversibility test result of 1-Fe₃O₄	45
Figure 4.20 Evaluation of Zn^{2+} in contaminated soil with proposed method..	47

Chapter 1 Introduction

1.1 General

Particular attention has been focused on heavy and transition metal (HTM) ions and their detection methods. Exposure to HTM through diverse pathways can lead to accumulation in the human body, causing severe illness (Sharma et al. 2007). In particular, zinc is an indispensable element as it plays an essential role in biological processes (e.g., protein synthesis, neurotransmission, and signal transduction) (Park et al 2008). However, the accumulation of zinc in the human body causes fatal organ failure, copper deficiency, stomach cramps, skin irritations, vomiting, nausea and anaemia (Plum et al. 2010; Kang et al. 2012). Thus, the detection and removal of Zn^{2+} in contaminated samples are of significant interest due to this cation's unique role in physiological functions and harmful effects to human body.

Currently, fluorescent sensors have been reported as powerful tools for detecting metal ions in water and biological samples, attributed to their high sensitivity and selectivity, as well as ease of operation (Sivaraman et al. 2014; Shanmugapriya et al. 2016). In particular, development of fluorescent sensors for Zn^{2+} have engaged great attention, due to the biological significance of Zn^{2+} ions. In general, fluorescent molecules are linked to Zn^{2+} -chelators such as dipicolylamine (DPA), bipyridine, cyclic polyamines, and etc (Xu et al. 2009; Xue et al. 2009; Sun et al. 2011; Wang et al 2012). However, most of the sensors exhibit a poor selectivity for Zn^{2+} ions over other metal ions.

Specially, there is difficulty in distinguishing Cd^{2+} and Zn^{2+} ions, owing to their similar binding properties (Masanta et al 2011; Xue et al. 2012). Recently, Xu et al. (2009) reported a Zn^{2+} -selective fluorescent sensor based on amide tautomerization of naphthalimide linked to DPA and this was used for detecting Zn^{2+} ions in human cells and zebrafish.

Compared to the detection of HTM present in contaminated water, that of HTM present in contaminated soil is considerably more difficult. Soil demonstrates potential to buff the contamination level of groundwater and river (Yong et al. 1990). HTM adsorbed on soil surfaces may leach into groundwater and stream water, which are important sources of drinking water (Chen et al. 2011). Thus, it is necessary to investigate the contamination of zinc in soil.

Conventional analytical methods widely employed for detecting HTM in soil samples include atomic adsorption spectrometry (Chen et al. 2001), inductively coupled plasma-mass spectroscopy (ICP-MS) (Rao et al. 2002), X-ray fluorescence spectrometry (Manceau et al. 2004), and laser-induced breakdown spectroscopy (Dell'Aglio et al. 2011). However, their applications are hindered by high cost and operational expertise, as well as lack of portability and time-consuming procedures (Al-Kady and Abdelmonem 2013). However, fluorescent sensors capable of detecting Zn^{2+} absorbed on soil have been rarely exploited. More recently, fluorescent-sensor-functionalized iron oxide nanoparticles (IOPs) have attracted immense attention, attributed to their sensing ability and strong magnetic property (Peng et al. 2011). Receptor-immobilized magnetic nanoparticles have some important

advantages as solid chemosensors and adsorbents in heterogeneous solid-liquid phases (Kang et al. 2012; Jung et al. 2011; Son et al. 2010; Park et al. 2010; Lee et al. 2009). First, such nanoparticles are readily synthesized by hydrolysis reaction which is a versatile technique that allows introduction of chemical functionalities. Second, immobilized receptors on inorganic nanoparticles can remove guest molecules (toxic metal ions and anions) from the pollutant solution. Third, magnetic nanoparticles can be easily isolated and controlled from pollutants by a small magnet and can be repeatedly utilized with suitable regenerative treatment. Magnetic nanoparticles can also provide efficient binding to guest molecules because of their high surface-to-volume ratio, which simply offers more contact area. Some functionalized IOPs have been developed for the selective detection and removal of metal ions (Wang et al. 2012; Kim et al. 2016; Zhang et al. 2015; Wang et al. 2006). Thus, we envisaged that the naphthalimide linked to DPA, combined with iron oxide nanoparticles, can be used for sensing, recovery, and removal of Zn^{2+} ions selectively in environmental pollution and biological specimens.

Herein, I presented a Zn^{2+} -selective fluorescent naphthalimide-functionalized Fe_3O_4 nanoparticles (**1- Fe_3O_4**), composed of naphthalimide-dipicolylamine (**1**) as a Zn^{2+} sensing unit and Fe_3O_4 as magnetic nanoparticles (NPs). The **1** consists of a naphthalimide fluorophore as the signaling unit, dipicolylamine (DPA) as the recognition site for Zn^{2+} , and dopamine as the group for immobilizing Fe_3O_4 .

1.2 Outline

This study is divided into five chapters.

Chapter 2 provides background of fluorescence chemosensor and their mechanism. The mechanism of fluorescence and quenching effect is explained.

Chapter 3 describes the experimental program about verification of proposed fluorescence chemosensor. In addition, synthesis process of proposed chemosensor is explained.

Chapter 4 mainly discuss the sensing characteristics of proposed fluorescence chemosensor based on the solution test results. Additionally, the application on contaminated soil is explained.

Chapter 5 summarized the sensing behavior of proposed fluorescence chemosensor and the results of application on contaminated soil.

Chapter 2 Background

2.1 Background of the Fluorescent Chemosensor

2.1.1 Fluorescence

Fluorescence is a specific characteristic of fluorophore. With specific molecular structure, conjugated molecules emit light followed by absorption light or other electromagnetic radiation. Each fluorophore can absorb specific wavelength that they can absorb. As shown in Figure 2.1, the electron of fluorophore at ground state level is excited by the photon to excited state level. Subsequently, by Kasha rule, the irradiated electron immediately vibrates and rotates down to the lowest level. Lastly, the electron drops down to ground state with the emission of a photon. This emitted light is known as fluorescence.

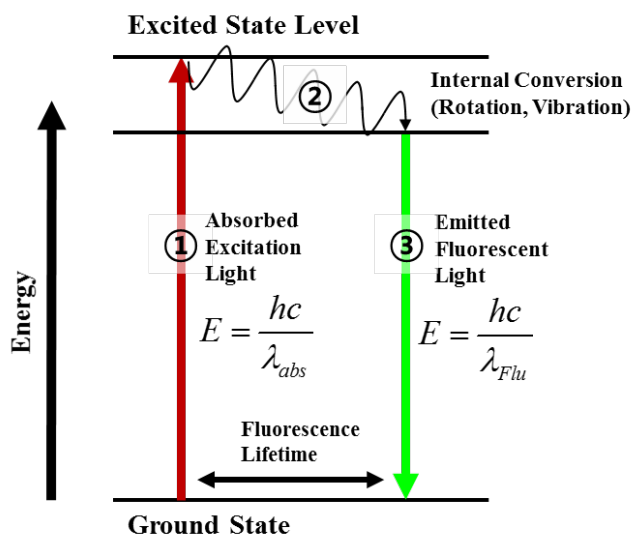


Figure 2.1 Mechanism of fluorescence

2.1.2 Photo-induced Electron Transfer

The intensity of fluorescence can be reduced by variety of method. The reduction in fluorescence intensity is called fluorescence quenching. One of the method that can quenches the fluorescence is photo-induced electron transfer(PET) which is widely used in fluorescence chemosensing field. PET-based fluorescence chemosensor mainly consist of three parts: fluorophore which is signal unit, Receptor that acts as a electron donor, and spacer that links fluorophore and receptor. When the electron of fluorophore is irradiated, the electron of fluorophore at highest occupied molecular orbital (HOMO) is transfered to the state of lowest unoccupied molecular orbital (LUMO). The HOMO energy level of receptor is higer than that of fluorophore and lower that LUMO of fluorophore. As a result, the electorn in HOMO of receptor transfers to the electron in HOMO of fluorophore that prohibits the electron in LUMO of fluorophore returning to the state of HOMO. This effect is called as PET effect that quenches the fluorescence.

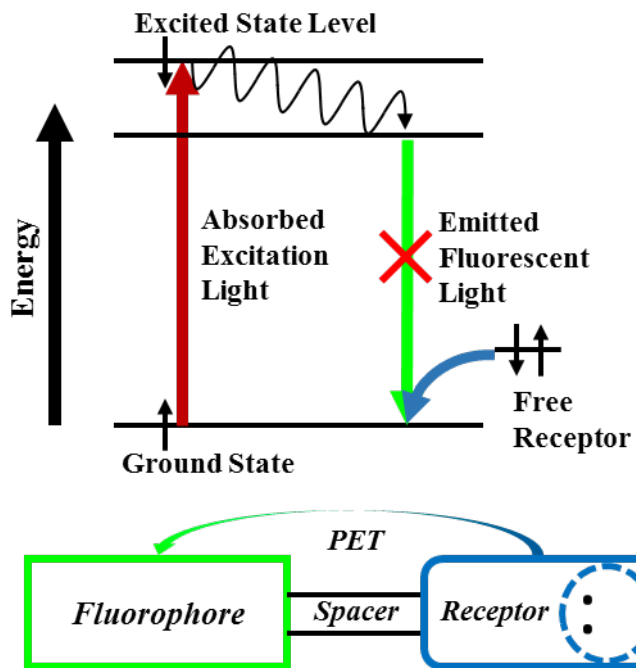


Figure 2.2 Mechanism photo-induced electron transfer.

2.1.3 Chelation Enhanced Fluorescence

Without any binds on receptor, the fluorescence chemosensor loses its own fluorescence intensity due to PET effect. But when the receptor binds target substance such as metal ion, the HOMO energy level of receptor changes to be lower than that of fluorophore. In other words, upon binding of target substance to the receptor, the PET effect is blocked, and the fluorescence is recovered. Above mentioned process is called as chelation enhanced fluorescence (CHEF).

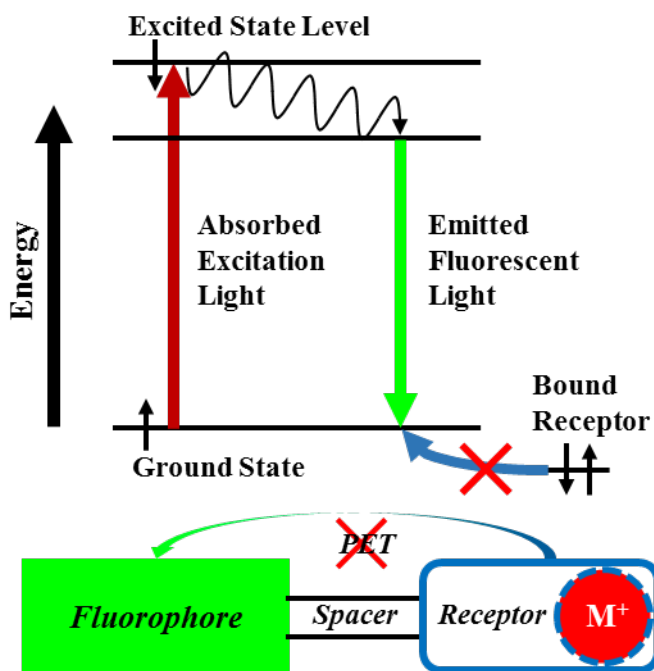


Figure 2.3 Mechanism of chelation enhanced fluorescence

Chapter 3 Experimental Program

3.1 Materials and instruments

All fluorescence and UV–Vis absorption spectra were recorded on Shimadzu RF-6000 and UV-2600 spectrophotometers, respectively. NMR spectra were recorded on a Varian instrument (400 MHz). Infrared (IR) spectra were recorded on a Shimadzu FTIR 8400S instrument in the range of 400–4000 cm^{-1} by the KBr pellet method. Transmission electron microscopy (TEM) images were recorded on a JEOL JEM-2100 TEM system operating at 200 kV (293 K) at an accelerating voltage of 100 kV and a working distance of 16 mm. Thermogravimetric analysis (TGA) measurements were performed on a TA Instruments Q-50 thermogravimetric analyzer.

3.2 Spectroscopic methods

Stock solutions of cationic compounds (chloride salts of Na^+ , K^+ , Zn^{2+} , Ca^{2+} , Mg^{2+} , Ba^{2+} , Cd^{2+} , Co^{2+} , Pb^{2+} , Hg^{2+} , Ni^{2+} , Cu^{2+} , Fe^{2+} , and Fe^{3+}) were prepared using deionized water. Stock solutions of synthetic compounds were prepared using DMSO. All spectra were collected in HEPES buffer (20 mM, pH = 7.4) containing 50% (v/v) of DMSO.

3.3 Determination of limit of detection for $\mathbf{1-Fe_3O_4}$

The limit of detection (LOD) was calculated using the general definition proposed by Gary and Winefordner et al. (1983). The LOD should correspond to the concentration as three times the standard deviation of 10 blank measurements. The LOD of $\mathbf{1-Fe_3O_4}$ was found to be 0.0345 ppb for Zn^{2+} . It was determined by analyzing four standard solutions of DMSO and 20 mM HEPES (pH 7.4, v/v = 50:50) containing 0.03, 0.15, 0.25, 0.35 ppb of Zn^{2+} , respectively.

3.4 Synthesis

3.4.1 Synthesis of iron-oleate complex

Metal–oleate complexes were prepared by the reaction between metal chlorides and sodium oleate. In a typical synthesis, 10.8 g of iron(III) chloride hexahydrate (98%, $\text{FeCl}_3 \cdot 6\text{H}_2\text{O}$, 40 mmol, Aldrich) and 36.5 g of sodium oleate (120 mmol, TCI, 95%) were first dissolved in a mixture of 80 mL of ethanol, 60 mL of distilled water, and 140 mL of hexane. Second, the resulting mixture was heated at 70 °C for 4 h. Upon reaction completion, the upper organic layer containing the iron–oleate complex was washed three times with 30 mL of distilled water, followed by concentration in vacuo, affording a waxy solid as the final product.

3.4.2 Synthesis of iron oxide nanocrystals

A typical procedure for synthesizing monodisperse iron oxide (Fe_3O_4) nanocrystals with a size of 12 nm is described as follows. First, the prepared iron–oleate complex (36 g, 40 mmol) and oleic acid (5.7 g, 20 mmol, Aldrich, 90%) were dissolved in 1-octadecene (200 g, Aldrich, 90%) at room temperature. Second, the reaction mixture was heated to 320 °C at a constant heating rate of 3.3 °C min^{-1} , followed by maintaining this heating temperature for 30 min. A noticeable reaction occurred when the reaction temperature reached 320 °C, and the initially transparent solution became turbid and brownish black. Finally, the reaction mixture

was cooled to room temperature, and ethanol (500 mL) was added to precipitate IOPs, which were then separated by centrifugation.

3.4.3 Synthesis of **1-Fe₃O₄**

Ligand-exchange reaction-based synthesis of **1-Fe₃O₄** particles was performed according to a previously reported study (Wei et al. 2012). In this method, 2-[2-(2-methoxyethoxy)ethoxy]acetic acid (MEAA) ligand was used as an intermediate compound for increasing the solubility of NPs. Briefly, ethanol was added to 75 μ L of NPs in the growth solution to the point of turbidity, followed by centrifugation and decantation, affording \sim 3 mg of a dry pellet; second, 100 μ L of neat MEAA ligand and 300 μ L of methanol were added to this dry pellet. Third, the mixture was stirred at 70 °C for 5 h, followed by precipitation with the successive addition of 0.8 mL of acetone and 3.2 mL of hexane. Finally, the mixture was centrifuged at 15000 rpm for 5 min, forming a clear supernatant, which was discarded. Then, the pellet was dispersed in a mixed solution of 3 mL of MeOH and 0.5 mL of DI water, followed by the addition of 30 mg of compound 1. The mixture was stirred again under N₂ at 70 °C for 12 h, followed by precipitation with the addition of 10 mL of acetone. The resulting mixture was centrifuged at 15000 rpm for 5 min, affording a transparent solution, which was discarded. Then, the pellet was dispersed in 3 mL of DMSO/HEPES buffer (1/1 v/v%, pH = 7.4, 10 mM) and sonicated for 10

min. The sample was further purified by centrifugation at 15000 rpm for 5 min.

3.4.4 Synthesis of 1-5

Compounds **1-4** were synthesized by following procedures. Compound **5** was prepared according to a previously published method (Lee et al. 2012).

3.4.5 Synthesis of 1

A mixture of **2** (30 mg, 0.06 mmol), 1-ethyl-3-(3-dimethylaminopropyl) carbodiimide (EDCI) (22 mg, 0.11 mmol), and DMAP (14 mg, 0.11 mmol) in dimethylformamide (DMF) (5 mL) was stirred under N₂ at room temperature for 30 min. Then, dopamine (16 mg, 0.08 mmol) was added to the reaction mixture, followed by stirring overnight under N₂. Upon reaction completion, the reaction mixture was diluted with ethyl acetate and washed with water. The collected organic layer was dried over anhydrous Na₂SO₄. After solvent removal, the product was purified by silica column chromatography using DCM/MeOH (v/v, 30:2) as the eluent, affording **1** (0.021g, 55%) as a yellowish oil. ESI-MS m/z [M+Na]⁺ calc. 658.254, obs. 659.2545. ¹H NMR (CD₃OD, 400 MHz): δ 2.51–2.57 (m, 2H); 2.66 (t, J = 8.0, 2H); 3.27 (d, J = 8.0, 2H); 3.62 (s, 2H); 4.06 (s, 4H); 4.27–4.31 (m, 2H); 6.46–6.51 (m, 1H); 6.59–6.67 (m, 1H); 7.19–7.23 (m, 2H); 7.46 (d, J = 7.6 Hz, 2H); 7.69–7.78 (m,

3H); 8.16–8.24 (m, 2H); 8.41 (d, J = 3.8 Hz, 4H); 8.74 (t, J = 8.9 Hz, 1H).
¹³C NMR (CD₃OD, 100 MHz): 174.0, 173.1, 165.6, 164.9, 159.7, 151.0, 146.9, 145.3, 141.3, 139.1, 133.7, 132.7, 130.1, 128.1, 125.8, 124.7, 124.0, 123.9, 121.7, 118.7, 118.5, 117.6, 117.1, 62.2, 60.9, 43.0, 37.8, 36.5, 34.0 ppm.

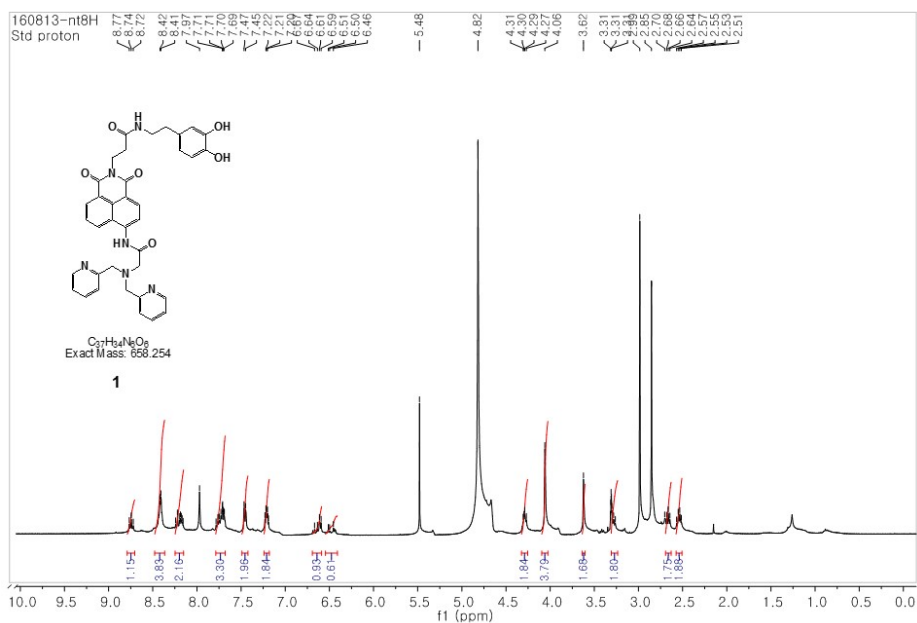


Figure 3.1 ¹H NMR spectrum of **1** in CD₃OD.

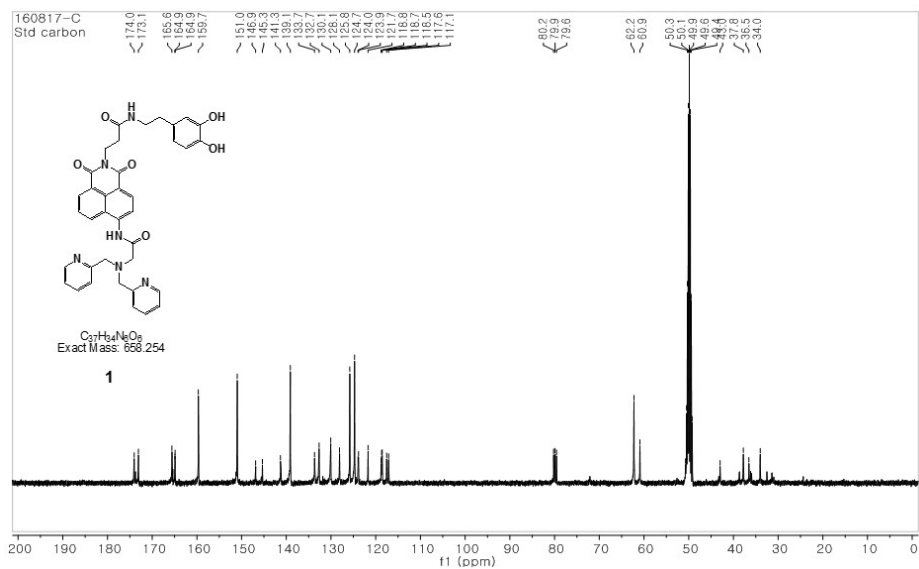


Figure 3.2 ^{13}C NMR spectrum of **1** in CD_3OD .

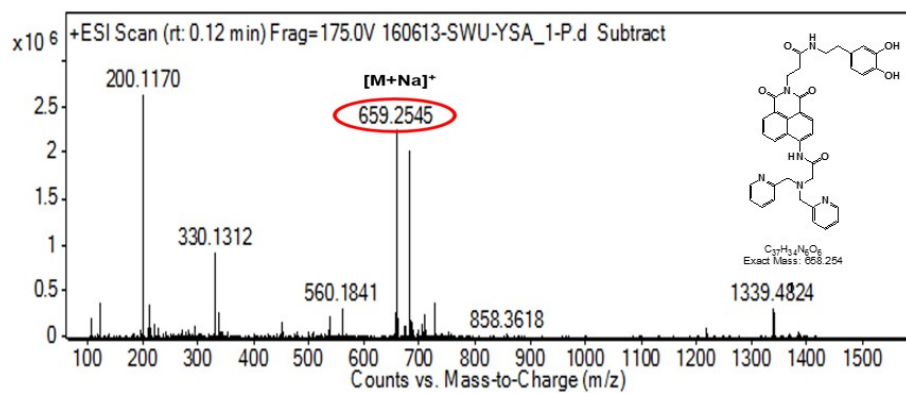


Figure 3.3 ESI-MS spectrum of **1**.

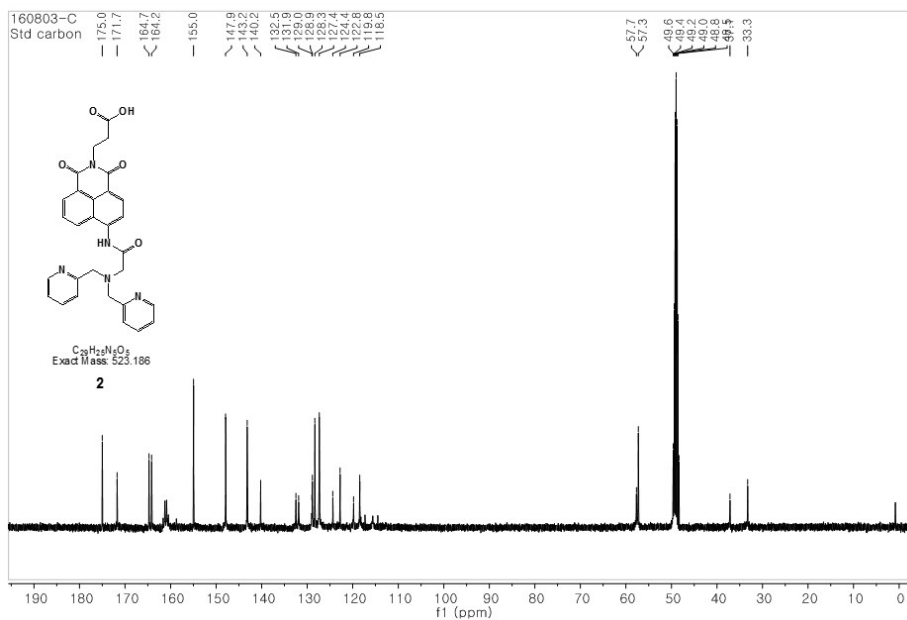


Figure 3.5 ^{13}C NMR spectrum of **2** in CD_3OD .

Line#:1 R.Time:0.517(Scan#:63)
 MassPeaks:730
 RawMode:Single 0.517(63) BasePeak:305.05(176311)
 BG Mode:None Segment 1 - Event 1

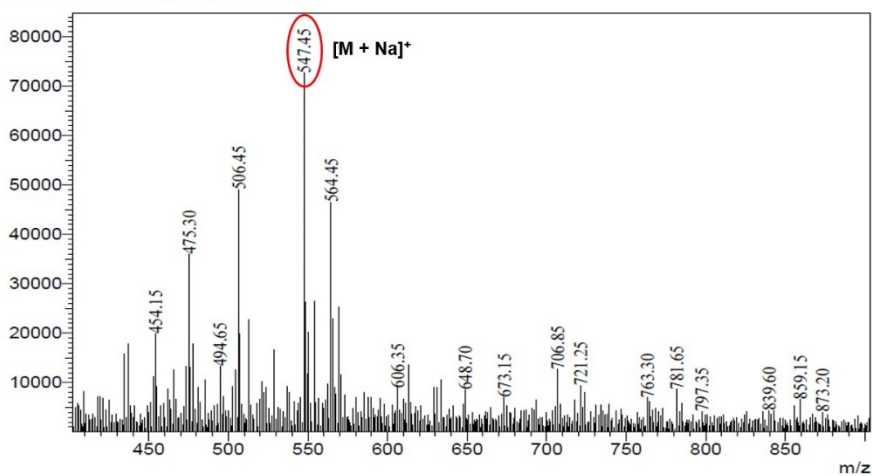


Figure 3.6 ESI-MS spectrum of **2**.

3.4.7 Synthesis 3

To a mixture of **4** (0.36 g, 0.86 mmol), DPA (0.16 mL, 1.23 mmol) and KI (0.21 g, 1.27 mmol) in CH₃CN (50 mL), N,N-diisopropylethylamine (DIPEA) (1.52 mL, 8.73 mmol) was added. The resulting solution was stirred for 24 h under reflux in nitrogen. Upon reaction completion, the solution was evaporated, and the product was dissolved in DCM and washed with water. The collected organic layer was dried over anhydrous Na₂SO₄. Finally, after solvent removal, the product was purified by silica column chromatography using DCM/MeOH (v/v, 40:1) as the eluent, affording **3** (0.42 g, 82%) as a dark brown oil. ESI-MS *m/z* [M+Na]⁺ calc. 581.2638, obs. 602.100. ¹H NMR (CDCl₃, 400 MHz): δ 1.43 (s, 9H); 2.70 (t, *J* = 8.0 Hz, 2H); 3.62 (s, 2H); 4.08 (s, 4H); 4.47 (t, *J* = 8.0 Hz, 2H); 7.14–7.17 (m, 2H); 7.31 (d, *J* = 7.7 Hz, 2H); 7.60–7.64 (m, 2H); 7.83–7.86 (m, 1H); 8.45 (d, *J* = 4.0 Hz, 2H); 8.59 (d, *J* = 8.3 Hz, 1H); 8.65–8.70 (m, 2H); 9.11 (d, *J* = 8.6 Hz, 1H); 11.77 (s, 1H). ¹³C NMR (CDCl₃, 100 MHz): 170.7, 170.5, 163.9, 163.3, 157.5, 149.4, 139.9, 136.7, 132.5, 131.0, 128.8, 128.3, 126.1, 123.4, 123.3, 122.6, 117.2, 116.8, 80.6, 60.5, 59.1, 36.0, 33.8, 27.9 ppm.

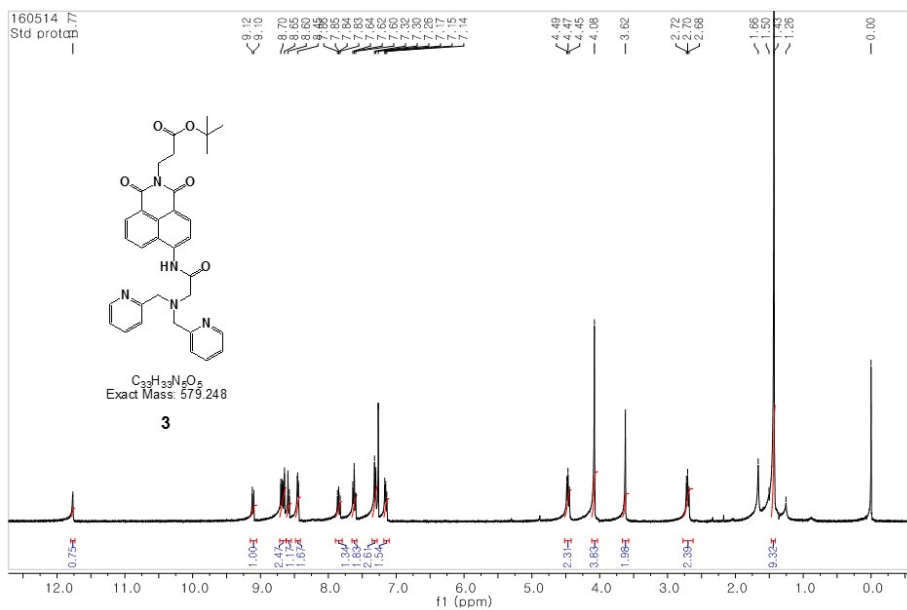


Figure 3.7 ^1H NMR spectrum of **3** in CDCl_3 .

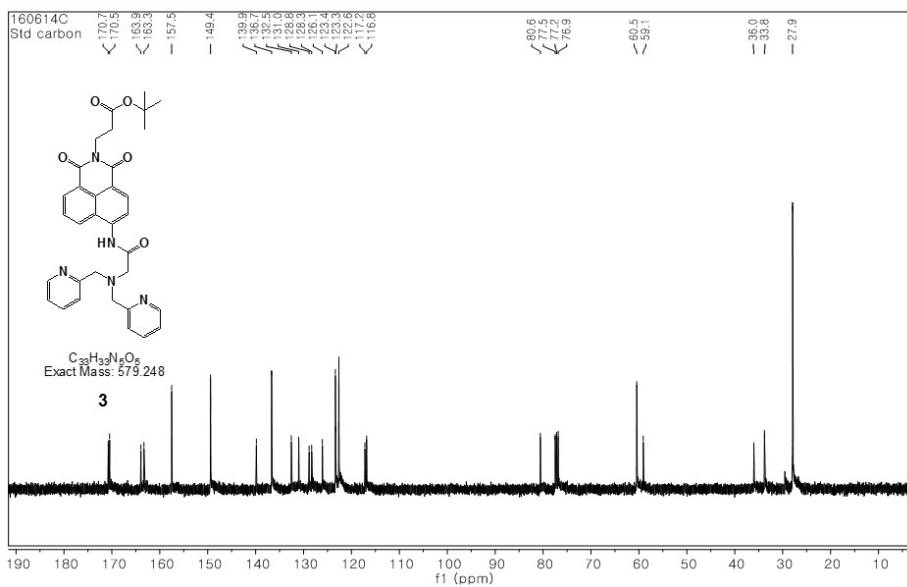


Figure 3.8 ^{13}C NMR spectrum of **3** in CDCl_3 .

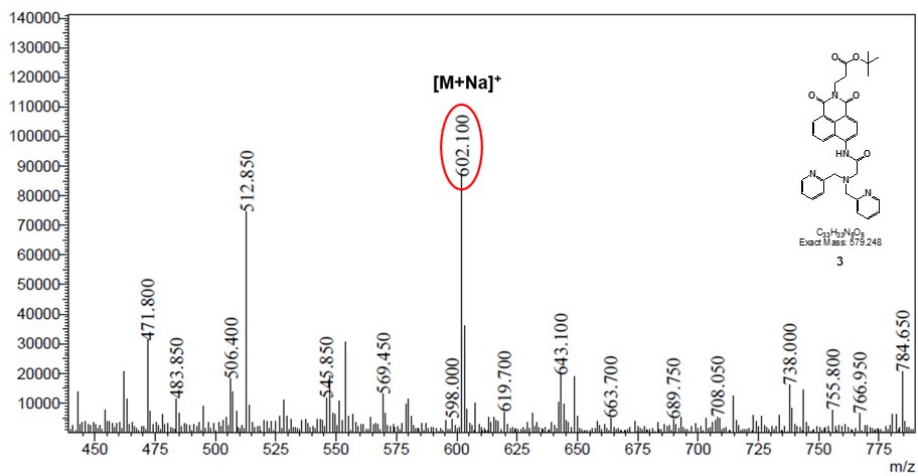


Figure 3.9 ESI-MS spectrum of **3**.

3.4.8 Synthesis of **4**

The **5** (0.5 g, 1.47 mmol) was mixed with chloroacetyl chloride (0.8 g, 1.47 mmol) and 4-dimethylaminopyridine (DMAP) (0.25 mL, 2.05 mmol) in 30 mL dry dichloromethane (DCM). The mixture was stirred in an ice bath for 5 h under N₂. Upon reaction completion, the solvent was evaporated, and the product was dissolved in DCM and washed with water. The collected organic layer was dried over anhydrous Na₂SO₄. Finally, after solvent removal, the product was purified by silica column chromatography using DCM/MeOH (v/v, 30:1) as the eluent, affording **4** (0.6 g, 98%) as a dark brown oil. ESI-MS m/z [M-H]⁻ calc. 416.1139, obs. 414.950. ¹H NMR (CDCl₃, 400 MHz): δ 1.42 (s, 9H); 2.69 (t, J = 8.0 Hz, 2H); 4.40 (s, 2H); 4.44 (t, J = 8.0 Hz, 2H); 7.81 (t, J = 8.0 Hz, 1H); 8.19 (d, J = 8.4 Hz, 1H); 8.45 (d, J = 8.2 Hz, 1H); 8.58–8.63 (m, 2H); 9.16 (s, 1H). ¹³C NMR (CDCl₃, 100 MHz): 170.6, 164.9, 163.4, 162.9, 137.4, 131.6, 131.1, 128.3, 126.8, 126.4, 123.8, 122.6, 119.5, 118.9, 80.9, 43.3, 36.2, 33.8, 27.9 ppm.

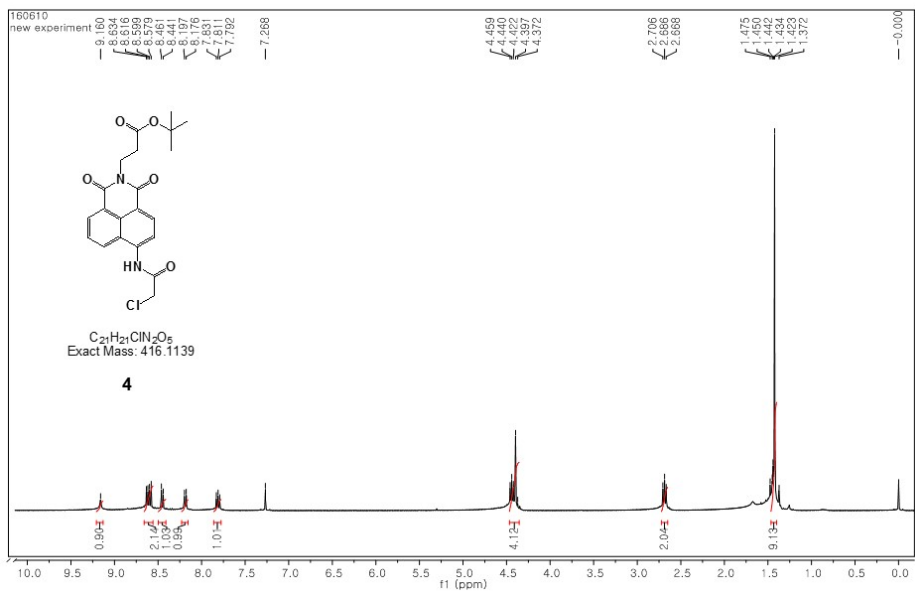


Figure 3.10 1H NMR spectrum of **4** in $CDCl_3$.

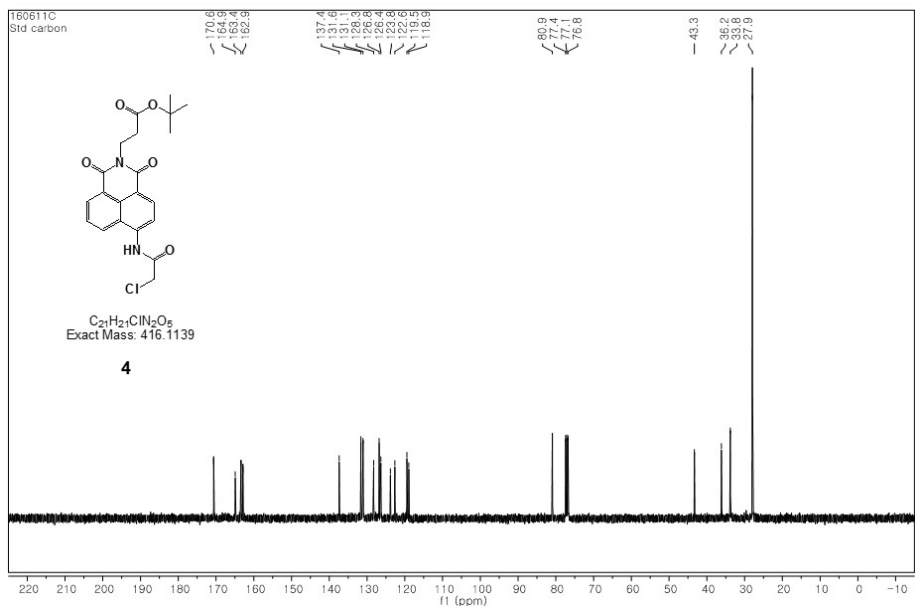


Figure 3.11 ^{13}C NMR spectrum of **4** in $CDCl_3$.

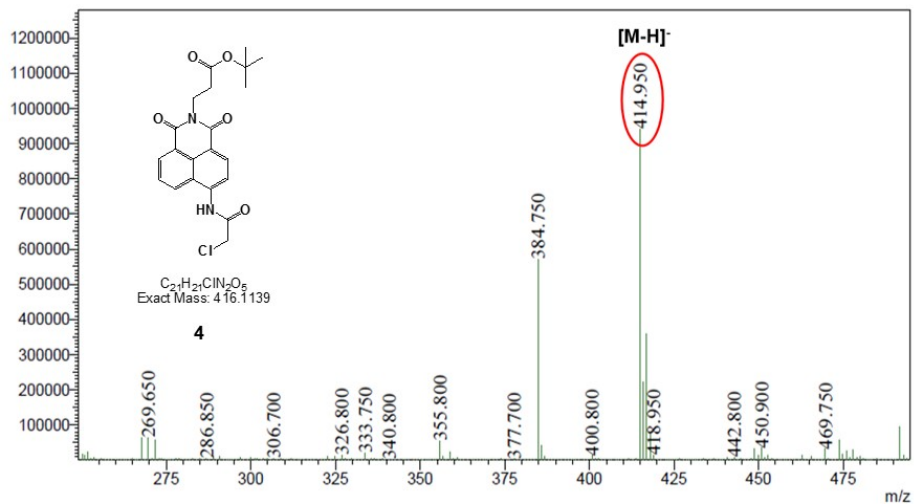


Figure 3.12 ESI-MS spectrum of **4**.

3.5 Soil sampling, spiking, and extraction

Surface soil samples were collected from the Gwanak Mountain area in South Korea; the soil samples were air-dried, ground, and sieved, yielding particles with a size of less than 2 mm. First, 15 mL of a 9000 mg/L zinc nitrate solution was added to 150 g of the parent soil samples (at a solid:liquid ratio of 1:10), furnishing a target concentration of approximately 900 mg/kg. Second, the soil and zinc nitrate solution mixture was incubated in a temperature–humidity chamber for 30 days. For extraction, 1.5 g of the incubated soil sample was treated with 15 mL of concentrated nitric acid at room temperature and kept overnight in a fume chamber. Next, 10 mL of the supernatant was collected, and 90 mL of distilled water was added to it. Subsequently, 5 mL of this diluted solution was neutralized to pH 7 using a 1 M NaOH solution. Finally, additional distilled water was added to attain a total volume of 50 mL. The Zn^{2+} concentration in the eluate extracted from soil sample was measured by fluorescent $1\text{-Fe}_3\text{O}_4$, as well as, ICP-MS.

Chapter 4 Experimental Results and Analysis

4.1 Synthesis and characterization of nanomagnet **1-Fe₃O₄**

The synthesis process of proposed **1-Fe₃O₄** is depicted in Figure 4.1. Compound **5** was synthesized according to a previously reported procedure (Xue et al. 2009). First, **5** was treated with chloroacetyl chloride in the presence of DMAP as the base, affording **4**, which was treated with DPA, DIPEA, and KI in CH₃CN, furnishing **3**. Subsequently, **3** was transformed to **2** in TFA/DCM. Next, **2** was coupled with dopamine in the presence of EDCI and DMAP in DMF, affording **1**. Finally, **1** was immobilized on the surface of Fe₃O₄ in methanol under reflux, affording fluorescent nanomagnet **1-Fe₃O₄**. All synthetic products were confirmed by ¹H NMR, ¹³C NMR, FTIR, and ESI-MS (Figure 2.1-2.12). **1-Fe₃O₄** was characterized by IR, TEM, and TGA. As shown in Figure 4.2, new strong peaks corresponding to **1** were observed in the IR spectrum of **1-Fe₃O₄**, indicating that **1** is strongly bound to Fe₃O₄ particles. TEM measurements confirmed that **1-Fe₃O₄** exhibits spherical morphology with a particle diameter of ca. 9 nm (Figure 4.3). These results indicate that **1** is successfully grafted on the Fe₃O₄ surface, accounting for ~16.03 wt% of **1-Fe₃O₄**, based on TGA result (Figure 4.4).

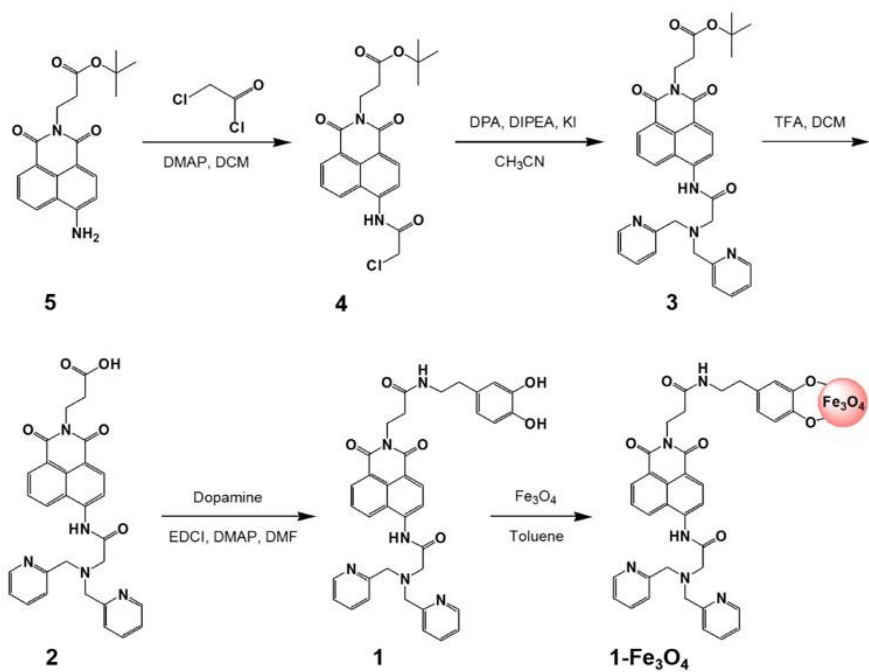


Figure 4.1 Synthesis of nanomagnet **1-Fe₃O₄**.

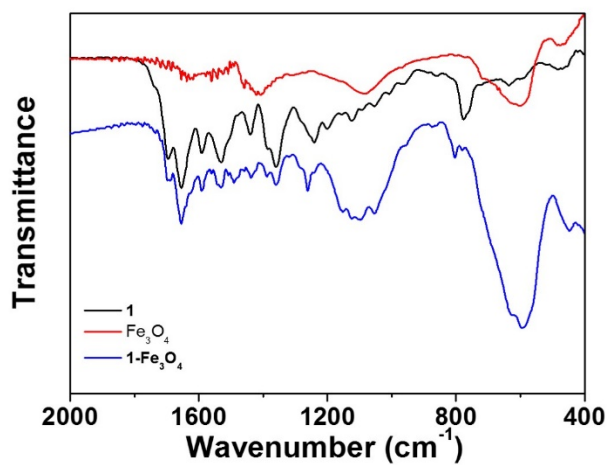


Figure 4.2 IR spectra of 1, Fe₃O₄, and 1-Fe₃O₄

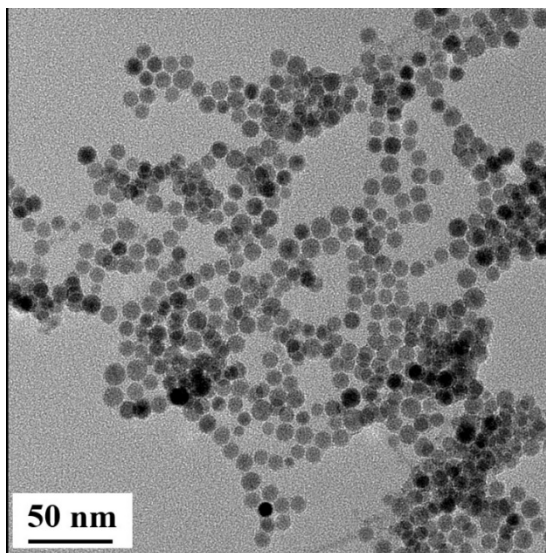


Figure 4.3 TEM image of 1-Fe₃O₄ particles.

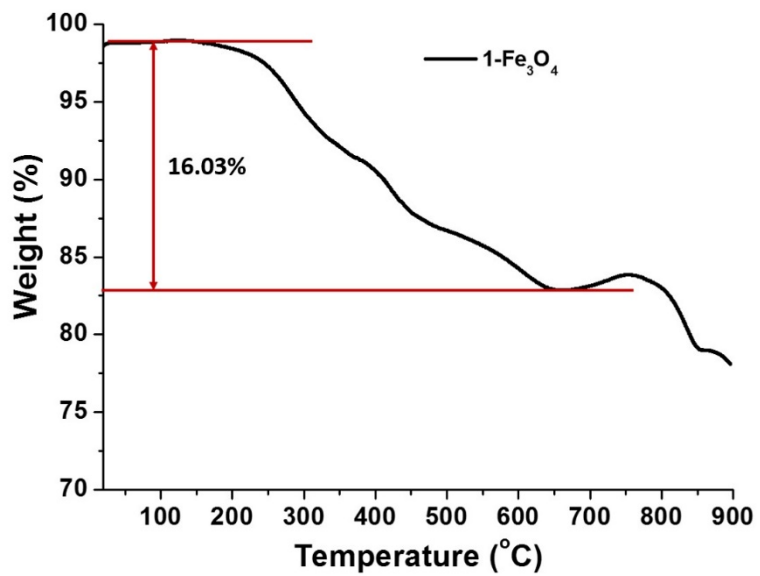


Figure 4.4 TGA curve of 1-Fe₃O₄

4.2 Spectroscopic analysis of the response of **2** to Zn^{2+} ions

Spectroscopic analysis was conducted with **2** to verify the selective of **2** toward Zn^{2+} . Additionally, considering field condition, pH titration test was conducted to verify the range of pH that the proposed **2** and **1-Fe₃O₄** can perform well. Further, detection range was determined by adding increasing amount of Zn^{2+} to the solution of **2** confirming linear change in fluorescence intensity at 527 nm. Lastly, Reversibility of **2** attributed by chelation was verified by adding excessive amount of Zn^{2+} and Ethylenediaminetetraacetic acid (EDTA) alternately.

4.2.1 Selectivity of **2** to Zn^{2+}

The sensing behavior of **1-Fe₃O₄** is dominated by the DPA-linked naphthalimide moiety. The fluorescence spectral change of **2** was first observed in presence of metal cations which can exist in soil leachate, such as Na^+ , K^+ , Zn^{2+} , Ca^{2+} , Mg^{2+} , Ba^{2+} , Cd^{2+} , Co^{2+} , Pb^{2+} , Hg^{2+} , Ni^{2+} , Cu^{2+} , Fe^{2+} , and Fe^{3+} , in HEPES buffer at pH 7.4 containing 50% (v/v) of DMSO. As shown in Figure 4.5, the spectral change of **2** toward Zn^{2+} in presence of other competitive metal ions can characterized into three types from the test results; 1) noncompetitive metal ions, 2) Competitive metal ions and 3) Quenching metal ions. From the results of Figure 4.5, the addition of K^+ , Na^+ , Ca^{2+} , Mg^{2+} , Ba^{2+} , Fe^{2+} and Fe^{3+} to the solution of **2** resulted marginal change in fluorescence. On the other hand, Upon addition of Zn^{2+} and

Hg²⁺ to a solution of **2** resulted fluorescence enhancement at 527nm with 8.8 and 2.3 fold, respectively. As shown in Figure 4.5 the fluorescence enhancement for Hg²⁺ was explicitly lower than that for Zn²⁺. Specifically, In presence of Cd²⁺ and Pb²⁺, **2** exhibited fluorescence spectral change at 471 nm and 550 nm. Due to the difference in spectra, Cd²⁺ and Pb²⁺ can be clearly discriminated from Zn²⁺ with naked eye (Figure 4.6). Lastly, fluorescence quenching was observed upon addition of Cu²⁺, Ni²⁺ and Co²⁺.

Similar investigation on fluorescent response of **2** to Zn²⁺ was also performed in presence of potential competitive metal ions. To the solution of **2** (10 μM), 100 μM of K⁺, Na⁺, Ca²⁺, Mg²⁺, Ba²⁺, Cd²⁺, Co²⁺, Pb²⁺, Hg²⁺, Ni²⁺, Cu²⁺, Fe²⁺, and Fe³⁺ were added. Subsequently 100 μM of Zn²⁺ was added to each solution. From the results (Figure 4.7 and 4.8) significant fluorescence enhancement at 527 nm was found in Cd²⁺, Pb²⁺, and Hg²⁺. Moreover, quenching metal ions such as Co²⁺ and Ni²⁺ gave a slight fluorescence enhancement upon addition of Zn²⁺. This results demonstrates that the **2** strongly binds with Zn²⁺ ions even in presence of Cd²⁺, Pb²⁺, Hg²⁺, Co²⁺ and Ni²⁺. To support the strongest affinity of **2** toward Zn²⁺, the association constants of **2** with Zn²⁺, Cd²⁺, Pb²⁺ and Hg²⁺ were calculated to be 1.55×10⁵ M⁻¹, 1.05×10⁵ M⁻¹, 4.20×10⁴ M⁻¹, and 4.90×10³ M⁻¹, respectively.

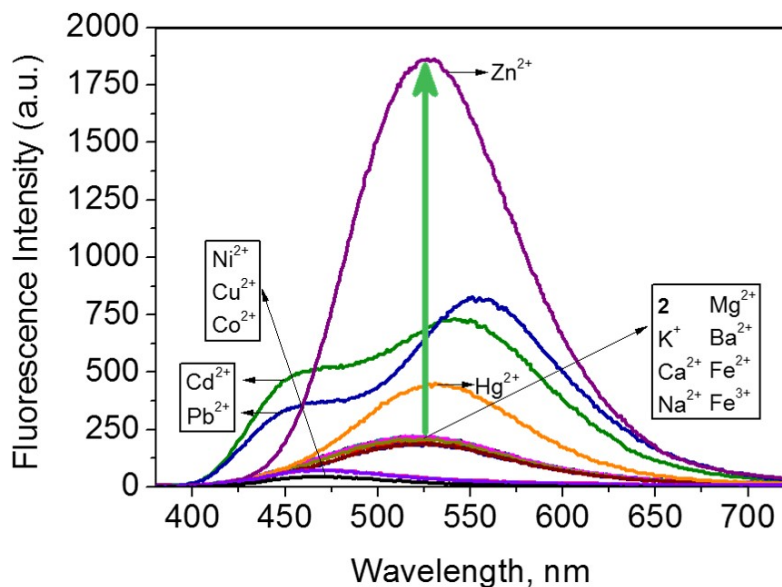


Figure 4.5 Fluorescence spectra of **2** (10 μ M) in the presence of various metal ions (K^+ , Na^+ , Ca^{2+} , Mg^{2+} , Ba^{2+} , Cd^{2+} , Co^{2+} , Pb^{2+} , Hg^{2+} , Ni^{2+} , Cu^{2+} , Zn^{2+} , Fe^{2+} , Fe^{3+} ; 10 equiv.) in an aqueous solution (DMSO/20 mM HEPES (pH 7.4) = 50:50). Excitation at 370 nm.

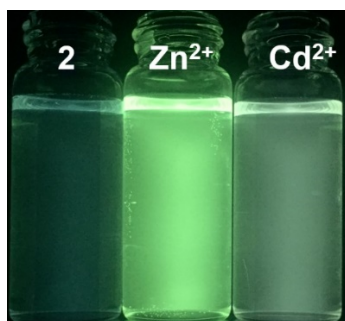


Figure 4.6 Visible emission observed for samples of **2**, **2/Zn²⁺**, and **2/Cd²⁺**.

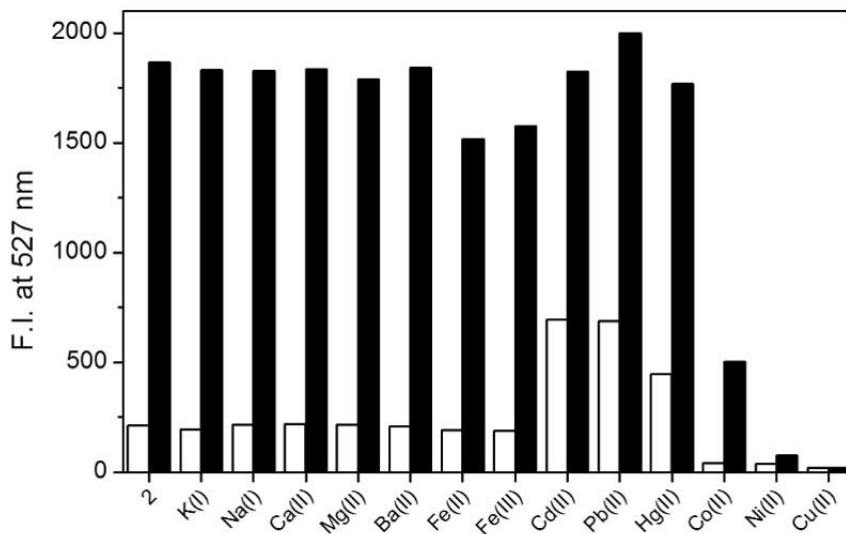


Figure 4.7 Fluorescence changes of **2** toward Zn^{2+} in the presence of various metal ions in HEPES buffer at pH 7.4 containing 50% (v/v) of DMSO. Excitation wavelength was 370 nm. White bars represent fluorescence intensity (F.I.) of **2** at 527 nm with the addition of metal cations (K^+ , Na^+ , Ca^{2+} , Mg^{2+} , Ba^{2+} , Fe^{2+} , Fe^{3+} , Cd^{2+} , Pb^{2+} , Hg^{2+} , Co^{2+} , Ni^{2+} , and Cu^{2+} ; 10 equiv.) to a solution of **2** ($10 \mu\text{M}$). Black bars represent F.I. of **2** at 527 nm with the subsequent addition of Zn^{2+} (10 equiv.) to the solutions of **2** containing various metal ions.

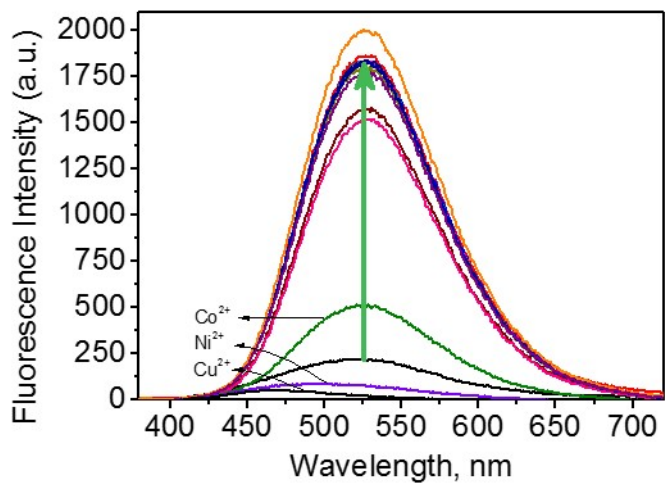


Figure 4.8 Fluorescence spectra of **2** (10 μM) complexed with Zn^{2+} (10 equiv.) with the addition of various metal ions (K^+ , Na^+ , Ca^{2+} , Mg^{2+} , Ba^{2+} , Cd^{2+} , Co^{2+} , Pb^{2+} , Hg^{2+} , Ni^{2+} , Cu^{2+} , Fe^{2+} , and Fe^{3+} ; 10 equiv.) in an aqueous solution (DMSO/20 mM HEPES (pH 7.4) = 50:50).

4.2.2 Zn²⁺ Titration Test of **2**

The sensing characteristic of **2** for Zn²⁺ was further investigate. The fluorescence intensity of **2** at 527 nm was observed against the function of Zn²⁺ concentration range of 0–14 μM. The fluorescence intensity of **2** at 527 nm linearly increased ($R^2=0.99$) over the Zn²⁺ concentration ranging from 0 to 7 μM. 10 μM of **2** was saturated with the addition of 7 μM of Zn²⁺, as shown in Figure 4.9. The quantum yield (Φ) of **2** was 0.08, while its quantum yield was 0.52 in the presence of Zn²⁺ (John et al. 1990). Additionally, Job's plot test was performed to verify the binding mode of **2** with Zn²⁺. As depicted in Figure 4.10, the job's plot results indicate that **2** forms 1:1 complex with Zn²⁺. The calculated association constant (K_a) of **2** for Zn²⁺ was $1.55 \times 10^5 \text{ M}^{-1}$ (Figure 4.11).

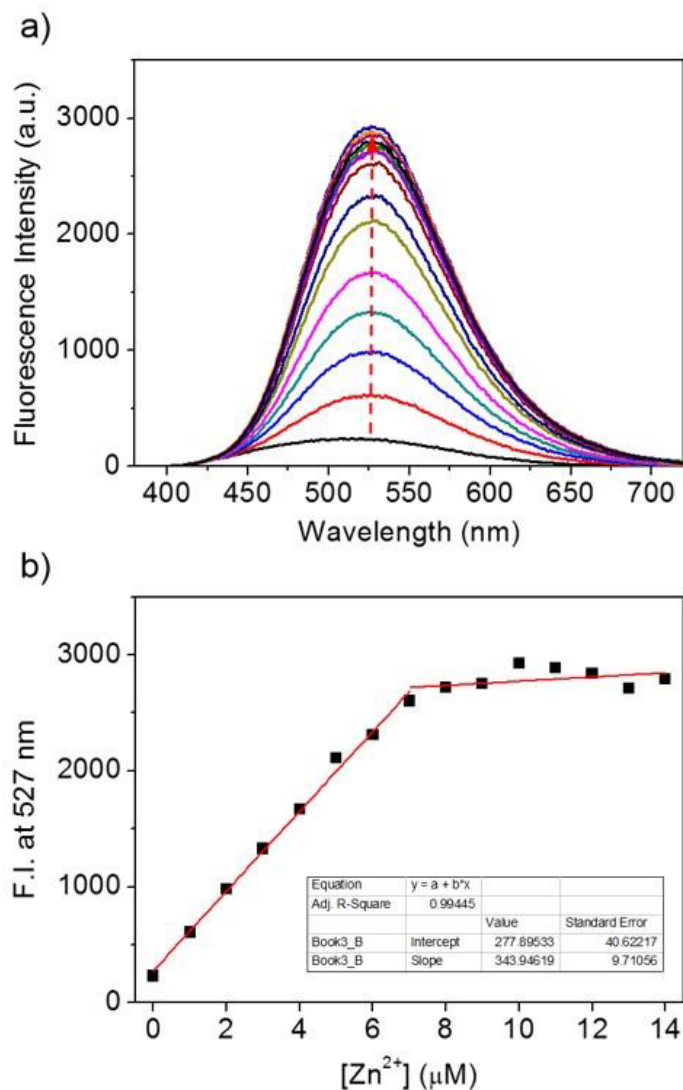


Figure 4.9 (a) Fluorescence spectra of **2** (10 μM) in presence of different concentrations of Zn^{2+} in HEPES buffer at pH 7.4 containing 50% (v/v) of DMSO. Excitation wavelength was 370 nm. (b) Plot of fluorescence intensity (F.I.) at 527 nm versus $[\text{Zn}^{2+}]$.

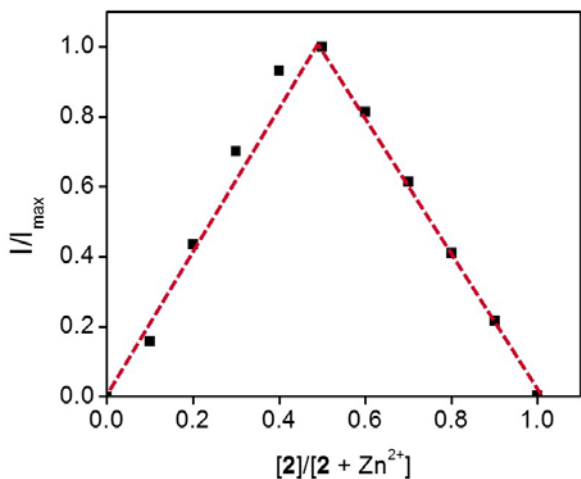


Figure 4.10 Job's plot for the complexation of **2** with Zn^{2+} in an aqueous solution (DMSO/20 mM HEPES (pH 7.4) = 1:1) with a total concentration of $10 \mu\text{M}$.

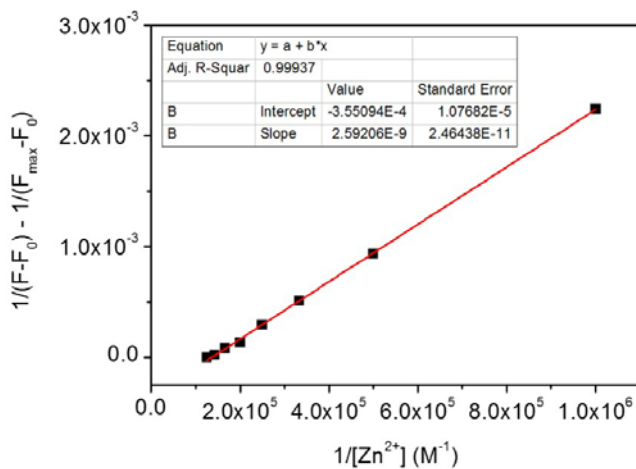


Figure 4.11 Benesi-Hildebrand plot of $1/(F - F_0) - 1/(F_{\max} - F_0)$ versus $1/[\text{Zn}^{2+}]$ for estimating the association constant (K_a) of **2** for Zn^{2+} .

4.2.3 pH Titration Test of 2

Considering field condition, The pH range of 2 that can selectively detect Zn^{2+} was investigated. The effect of pH on detection ability of 2 for Zn^{2+} was investigated in the pH range of 1 to 11. As shown in Figure 4.12, explicit amount of increase in fluorescence was found at the range from pH 4 to pH 11. This result implies that 2 can detect Zn^{2+} minimizing complicated pretreatment.

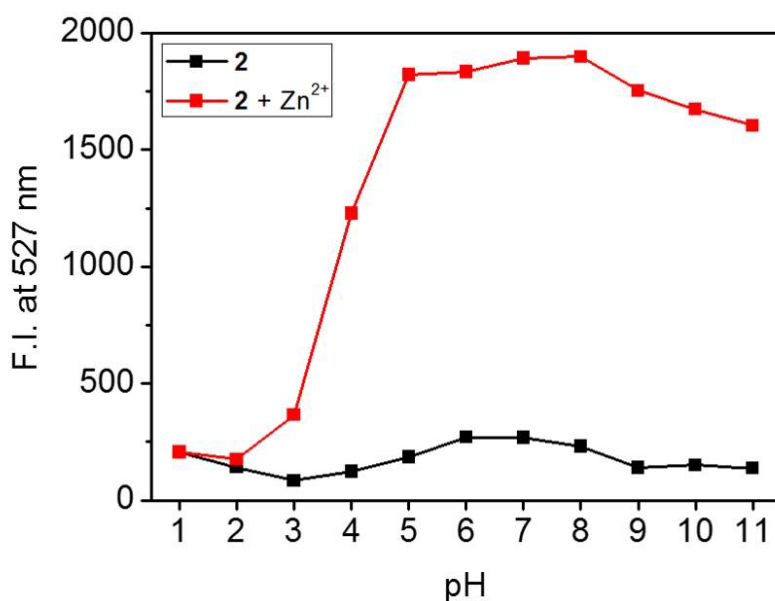


Figure 4.12 Fluorescence changes of 2 in solutions with different pH. Excitation wavelength was 370 nm. Black line represents the fluorescence intensity (F.I.) of 2 (10 μ M) at 527 nm. Red line represents the F.I. of 2 (10 μ M) at 527 nm in the presence of Zn^{2+} (10 equiv.).

4.2.4 Reversibility Test of **2**

Reversibility of **2** was investigated by adding excessive amount of Zn^{2+} and EDTA alternately. As shown in Figure 4.13, upon addition of Zn^{2+} , the fluorescence intensity at 527 nm increased. Subsequent addition of EDTA which well known as strong chelation reagent quenches the fluorescence. This result proves that the **2** is chelation based detection method. Additionally, by linking **2** onto Fe_3O_4 nanoparticle, the probe can be reused after treating with EDTA.

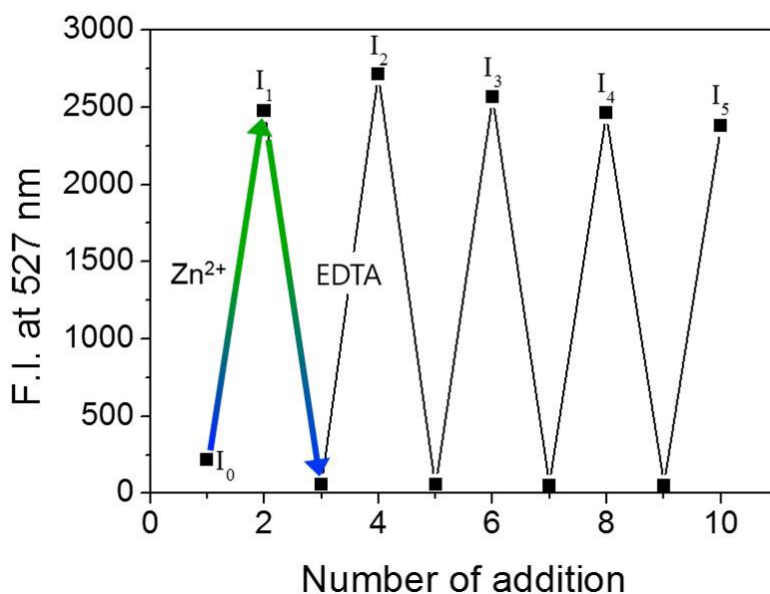


Figure 4.13 Reversible fluorescence change of **2** between Zn^{2+} and EDTA in HEPES buffer at pH 7.4 containing 50% (v/v) of DMSO. Excitation wavelength was 370 nm.

4.3 Spectroscopic analysis of the response of **1-Fe₃O₄** to **Zn²⁺**

Spectroscopic analysis was conducted with **1-Fe₃O₄** to verify the selective of **2** toward **Zn²⁺**. Additionally, reaction time of **1-Fe₃O₄** with **Zn²⁺** was investigated. Further, detection range was determined by adding increasing amount of **Zn²⁺** to the solution of **1-Fe₃O₄** confirming linear change in fluorescence intensity at 527 nm. Lastly, Reversibility of **2** attributed by chelation was verified by adding excessive amount of **Zn²⁺** and Ethylenediaminetetraacetic acid (EDTA) alternately.

4.3.1 Selectivity of **1-Fe₃O₄** to **Zn²⁺**

Weak fluorescence was observed at 527 nm (excitation: 370 nm) for **1-Fe₃O₄**, similar to that observed for **2** (Fig. 4.14). For investigating the metal sensing behavior of **1-Fe₃O₄**, the fluorescence change of **1-Fe₃O₄** was monitored in the presence of various metal ions (**K⁺**, **Na⁺**, **Zn²⁺**, **Ca²⁺**, **Mg²⁺**, **Ba²⁺**, **Cd²⁺**, **Co²⁺**, **Pb²⁺**, **Hg²⁺**, **Ni²⁺**, **Cu²⁺**, **Fe²⁺**, **Fe³⁺**) in HEPES buffer at pH7.4 containing 50% (v/v) of DMSO. As shown in figure 4.14, a marked emission enhancement was observed with the addition of **Zn²⁺** (~11-fold), while no significant change in fluorescence intensity was observed for other metal ions. Furthermore, competition experiments revealed that the fluorescence enhancement of **1-Fe₃O₄** by **Zn²⁺** is not affected by the presence of potential competitive metal ions, except for

Co^{2+} , Cu^{2+} , and Ni^{2+} (Figure 4.15), which can slightly interfere with Zn^{2+} -induced fluorescence enhancement.

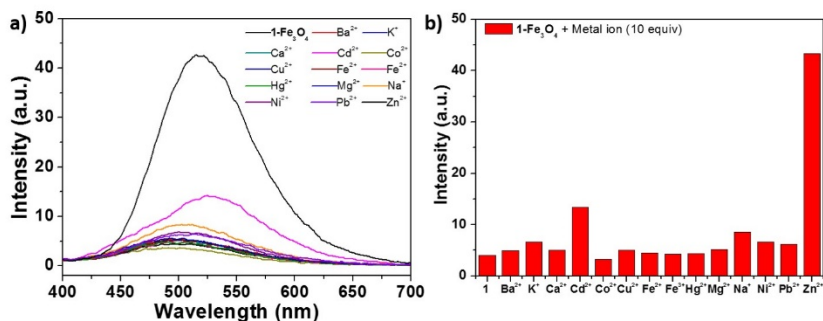


Figure 4.14 (a) Fluorescence spectra of **1-Fe₃O₄** (0.33 wt%) in the presence of various metal ions (K^+ , Na^+ , Ca^{2+} , Mg^{2+} , Ba^{2+} , Cd^{2+} , Co^{2+} , Pb^{2+} , Hg^{2+} , Ni^{2+} , Cu^{2+} , Zn^{2+} , Fe^{2+} , Fe^{3+} ; 10 equiv.) in aqueous solution (DMSO/20 mM HEPES (pH 7.4) = 50:50). Excitation at 370 nm. (b) Graph indicating the fluorescence intensity of **1-Fe₃O₄** in the presence of various metal ions.

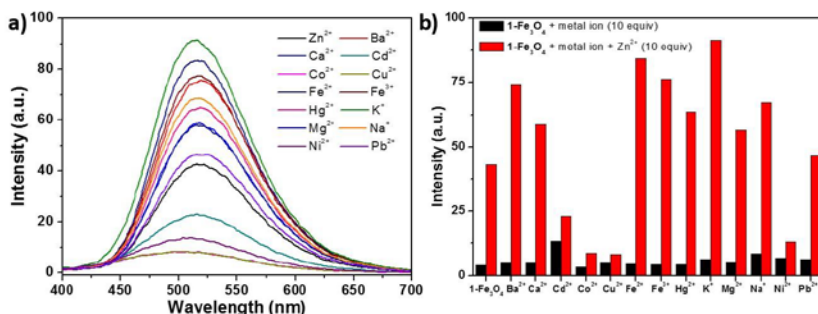


Figure 4.15 (a) Fluorescence spectra of **1-Fe₃O₄** (0.33 wt%) complexed with Zn²⁺ (10 equiv.) with the addition of metal cations (K⁺, Na⁺, Ca²⁺, Mg²⁺, Ba²⁺, Cd²⁺, Co²⁺, Pb²⁺, Hg²⁺, Ni²⁺, Cu²⁺, Fe²⁺, and Fe³⁺; 10 equiv.) in an aqueous solution (DMSO/20 mM HEPES (pH 7.4) = 50:50). Excitation wavelength was 370 nm. (b) Graph indicating the fluorescence intensity of noncomplexed **1-Fe₃O₄** (0.33 wt%, black bars) and that of its complex with Zn²⁺ (10 equiv., red bars) in the presence of various metal cations (10 equiv.) in HEPES buffer (pH 7.4) containing 50% (v/v) of DMSO.

4.3.2 Response Time of $1\text{-Fe}_3\text{O}_4$ to Zn^{2+}

For investigating the response time of $1\text{-Fe}_3\text{O}_4$ for sensing Zn^{2+} , fluorescence spectra were recorded at various elapsed times with the addition of Zn^{2+} (10 equiv., i.e., $50\ \mu\text{M}$) to a solution of $1\text{-Fe}_3\text{O}_4$ (Figure 4.16). Results indicated that the sensing response time of $1\text{-Fe}_3\text{O}_4$ with the addition of Zn^{2+} was maintained constant within 10 min.

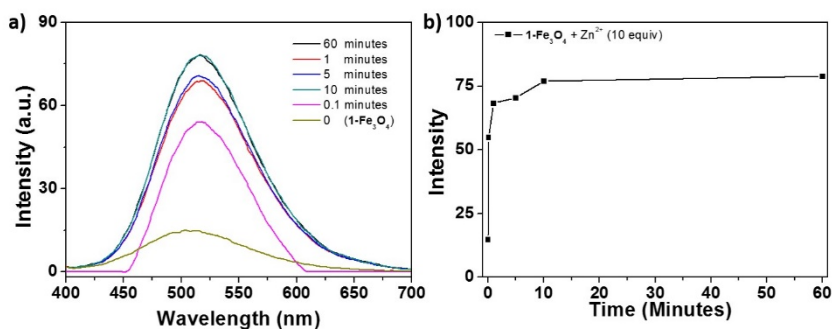


Figure 4.16 (a) Time-dependent fluorescence spectra of $1\text{-Fe}_3\text{O}_4$ (0.33 wt%) with the addition of Zn^{2+} (10 equiv.) in an aqueous solution (DMSO/20 mM HEPES (pH 7.4) = 50:50). (b) Plot of the fluorescence intensity of $1\text{-Fe}_3\text{O}_4$ (0.33 wt%) with Zn^{2+} (10 equiv.) as a function of time.

4.3.3 Zn²⁺ Titration Test of 1-Fe₃O₄

The fluorescence intensity of **1-Fe₃O₄** linearly increased as a function of Zn²⁺ concentration ($R^2 = 0.99$) in the range of 0–20 μM in HEPES buffer at pH 7.4 containing 50% (v/v) of DMSO (Figure 4.17). The limit of detection (LOD) of **1-Fe₃O₄** for Zn²⁺ was determined as 0.0345 ppb (Figure 4.18). The LOD was calculated by using following equation (Gray and Winefordner 1983; Mun et al 2016)

$$\text{LOD} = 3 \times \sigma/s$$

where σ is the standard deviation of the blank measurements, s is the slope of the calibration plot. Such an excellent sensitivity implied that **1-Fe₃O₄** can effectively detect even trace amounts of Zn²⁺ in contaminated samples.

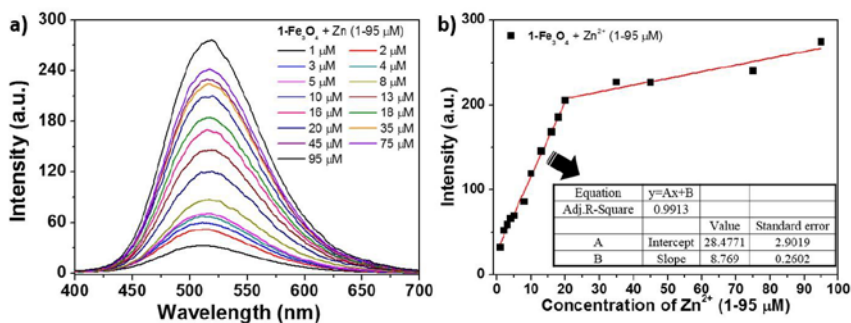


Figure 4.17 (a) Fluorescence spectra of **1-Fe₃O₄** (0.33 wt%) with different concentrations of Zn²⁺ in HEPES buffer at pH 7.4 containing 50% (v/v) of DMSO. Excitation wavelength was 370 nm. (b) Plot of fluorescence intensity (F.I.) at 527 nm versus [Zn²⁺].

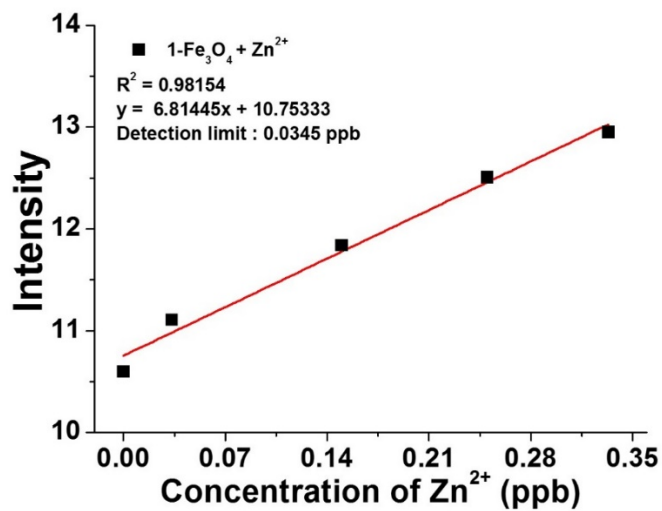


Figure 4.18 Plot of fluorescence intensity of **1-Fe₃O₄** (0.33 wt%) in the presence of 0.00–0.35 ppb of Zn²⁺ in an aqueous solution (DMSO/20 mM HEPES (pH 7.4) = 50:50).

4.4.4 Reversibility Test of 1-Fe₃O₄

The reusability of **1-Fe₃O₄** was confirmed by the use of EDTA (Figure 4.19 (a)). In addition, as shown in Figure 4.19 (b), the **1-Fe₃O₄**-Zn²⁺ complex was successfully separated using a magnet. Thus, **1-Fe₃O₄** is confirmed to be a simple, recyclable, and convenient system for detecting and removing trace amounts of Zn²⁺ in polluted environments.

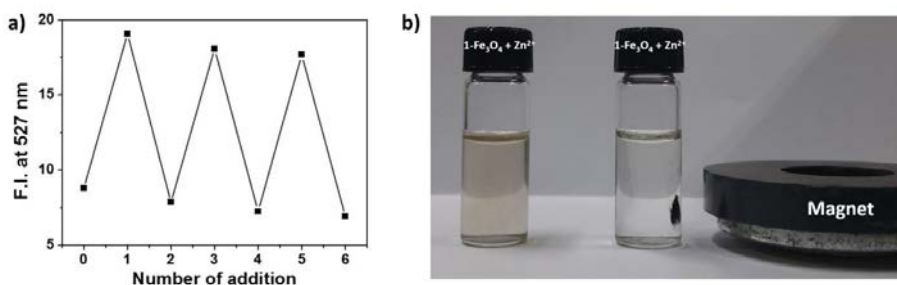


Figure 4.19 (a) Reversible fluorescence change of **1-Fe₃O₄** between Zn²⁺ and EDTA in HEPES buffer at pH 7.4 containing 50% (v/v) of DMSO. Excitation wavelength was 370 nm. (b) Photograph showing the separation of **1-Fe₃O₄** using a magnet in HEPES buffer at pH 7.4 containing 50% (v/v) of DMSO.

4.4 Detection of Zn^{2+} in soil samples

The detection ability of **1-Fe₃O₄** for Zn^{2+} present in contaminated soil was investigated. For this test, soil was treated with zinc nitrate and incubated for 30 days. Next, this incubated soil was treated with concentrated nitric acid, and a test solution was extracted. For the quantitative analysis of Zn^{2+} , the fluorescence change of **1-Fe₃O₄** in a solution extracted from the contaminated soil was evaluated. Based on the calibration curve in Figure 4.20, the Zn^{2+} concentration was found to be 6.3 μM ; this value is comparable to that obtained from ICP-MS (5.9 μM). Thus, **1-Fe₃O₄** demonstrates potential for the qualitative and quantitative detection of Zn^{2+} present in contaminated soil without any interference from other environmentally relevant metal ions. Furthermore, **1-Fe₃O₄** can be utilized as an efficient medium for detecting Zn^{2+} in various environmental samples.

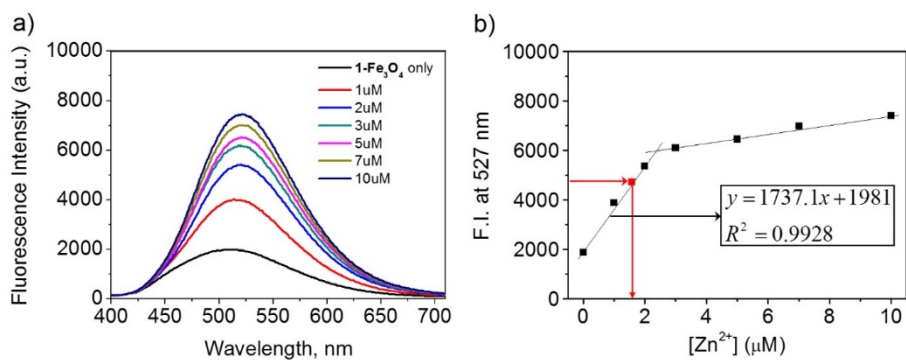


Figure 4.20 (a) Fluorescence spectra of **1-Fe₃O₄** (0.16 wt%) in the presence of different concentrations of Zn²⁺ in HEPES buffer at pH 7.4 containing 50% (v/v) of DMSO. Excitation wavelength was 370 nm. (b) Plot of fluorescence intensity (F.I.) at 527 nm versus [Zn²⁺]. Red dot indicated a fluorescence enhancement of **1-Fe₃O₄** collected from the eluate (4-fold dilution) extracted from soil sample.

Chapter 5 Conclusions

In summary, a hybrid nanomagnet **1-Fe₃O₄** functionalized with dopamine–naphthalimide–DPA (**1**), which can detect Zn²⁺, was prepared; significant increase in fluorescence was observed at 527 nm. This **1-Fe₃O₄** nanomagnet selectively detected Zn²⁺ in the presence of other metal ions, and the amount of Zn²⁺ in the aqueous solution was quantified by fluorescence spectrometry. **1-Fe₃O₄** exhibited an excellent limit of detection of 0.0345 ppb. In addition, the reusability of **1-Fe₃O₄** was confirmed by the use of EDTA, and the **1-Fe₃O₄-Zn²⁺** complex was successfully separated from aqueous media using a magnet. Furthermore, the qualitative and quantitative detection and removal of Zn²⁺ present in contaminated soil samples were possible without any interference from other environmentally relevant metal ions. These findings thus highlight that **1-Fe₃O₄** is a novel fluorescent sensors grafted on the surface of magnetic nanomaterials for the sensing, recovery, and removal of Zn²⁺ ions in environmental pollution and biological specimens.

- A reusable naphthalimide-functionalized nanomagnet was synthesized.
- The fluorescent nanomagnet exhibited high selectivity for Zn²⁺.
- The fluorescent nanomagnet exhibited an excellent limit of detection of 0.0345 ppb.
- The removal of Zn²⁺ was achieved by simple separation using a magnet.

Bibliography

Al-Kady, A. S., & Abdelmonem, F. I. (2013). Highly sensitive and selective spectrophotometric detection of trace amounts of Hg 2+ in environmental and biological samples based on 2, 4, 7-triamino-6-phenylpteridine. *Sensors and Actuators B: Chemical*, 182, 87-94.

Chen, J., & Teo, K. C. (2001). Determination of cadmium, copper, lead and zinc in water samples by flame atomic absorption spectrometry after cloud point extraction. *Analytica Chimica Acta*, 450(1), 215-222.

Chen, T. B., Wong, J. W. C., Zhou, H. Y., & Wong, M. H. (1997). Assessment of trace metal distribution and contamination in surface soils of Hong Kong. *Environmental pollution*, 96(1), 61-68.

Dell'Aglio, M., Gaudiuso, R., Senesi, G. S., De Giacomo, A., Zaccone, C., Miano, T. M., & De Pascale, O. (2011). Monitoring of Cr, Cu, Pb, V and Zn in polluted soils by laser induced breakdown spectroscopy (LIBS). *Journal of Environmental Monitoring*, 13(5), 1422-1426.

John, H. P. (1990). The UV-visible absorption and fluorescence of some substituted 1, 8-naphthalimides and naphthalic anhydrides. *Journal of the Chemical Society, Perkin Transactions 2*, (5), 837-842.

Jung, J. H., Lee, J. H., & Shinkai, S. (2011). Functionalized magnetic nanoparticles as chemosensors and adsorbents for toxic metal ions in environmental and biological fields. *Chemical Society Reviews*, 40(9), 4464-4474.

Kang, G., Son, H., Lim, J. M., Kweon, H. S., Lee, I. S., Kang, D., & Jung, J. H. (2012). Functionalized Fe₃O₄ nanoparticles for detecting zinc ions in living cells and their cytotoxicity. *Chemistry—A European Journal*, 18(19), 5843-5847.

Kim, K. T., Jung, H. S., Ahn, J., Choi, Y., Jung, J. H., Park, J. (2016). Selective detection of Hg²⁺ using fluorescent rhodamine-functionalized Fe₃O₄ nanoparticles. *RSC Advances*, 6(83), 79405-79409.

Lee, H. Y., Bae, D. R., Park, J. C., Song, H., Han, W. S., & Jung, J. H. (2009). A Selective Fluoroionophore Based on BODIPY-functionalized Magnetic Silica Nanoparticles: Removal of Pb²⁺ from Human Blood. *Angewandte Chemie*, 121(7), 1265-1269..

Lee, M. H., Han, J. H., Kwon, P. S., Bhuniya, S., Kim, J. Y., Sessler, J. L., ... & Kim, J. S. (2012). Hepatocyte-targeting single galactose-appended naphthalimide: a tool for intracellular thiol imaging in vivo. *Journal of the American Chemical Society*, 134(2), 1316-1322.

Long, G. L., & Winefordner, J. D. (1983). Limit of detection. A closer look at the IUPAC definition. *Analytical Chemistry*, 55(7), 712A-724A.

Manceau, A., Marcus, M. A., Tamura, N., Proux, O., Geoffroy, N., & Lanson, B. (2004). Natural speciation of Zn at the micrometer scale in a clayey soil using X-ray fluorescence, absorption, and diffraction. *Geochimica et Cosmochimica Acta*, 68(11), 2467-2483.

Masanta, G., Lim, C. S., Kim, H. J., Han, J. H., Kim, H. M., & Cho, B. R. (2011). A mitochondrial-targeted two-photon probe for zinc ion.

Journal of the American Chemical Society, 133(15), 5698-5700.

Mun, G., Jung, S. H., Ahn, A., Lee, S. S., Choi, M. Y., Kim, D. H., ... & Jung, J. H. (2016). Fluorescence imaging for Fe³⁺ in Arabidopsis by using simple naphthalene-based ligands. *RSC Advances*, 6(59), 53912-53918.

Park, S. Y., Yoon, J. H., Hong, C. S., Souane, R., Kim, J. S., Matthews, S. E., & Vicens, J. (2008). A pyrenyl-appended triazole-based calix [4] arene as a fluorescent sensor for Cd²⁺ and Zn²⁺. *The Journal of organic chemistry*, 73(21), 8212-8218.

Park, M., Seo, S., Lee, I. S., & Jung, J. H. (2010). Ultraefficient separation and sensing of mercury and methylmercury ions in drinking water by using aminonaphthalimide-functionalized Fe₃O₄@ SiO₂ core/shell magnetic nanoparticles. *Chemical Communications*, 46(25), 4478-4480.

Peng, X., Wang, Y., Tang, X., & Liu, W. (2011). Functionalized magnetic core-shell Fe₃O₄@ SiO₂ nanoparticles as selectivity-enhanced chemosensor for Hg (II). *Dyes and Pigments*, 91(1), 26-32.

Plum, L. M., Rink, L., & Haase, H. (2010). The essential toxin: impact of zinc on human health. *International journal of environmental research and public health*, 7(4), 1342-1365.

Rao, K. S., Balaji, T., Rao, T. P., Babu, Y., & Naidu, G. R. K. (2002). Determination of iron, cobalt, nickel, manganese, zinc, copper, cadmium and lead in human hair by inductively coupled plasma-atomic emission spectrometry. *Spectrochimica Acta Part B: Atomic*

Spectroscopy, 57(8), 1333-1338.

Sharma, R. K., Agrawal, M., & Marshall, F. (2007). Heavy metal contamination of soil and vegetables in suburban areas of Varanasi, India. *Ecotoxicology and environmental safety*, 66(2), 258-266.

Son, H., Lee, H. Y., Lim, J. M., Kang, D., Han, W. S., Lee, S. S., & Jung, J. H. (2010). A Highly Sensitive and Selective Turn-On Fluorogenic and Chromogenic Sensor Based on BODIPY-Functionalized Magnetic Nanoparticles for Detecting Lead in Living Cells. *Chemistry—A European Journal*, 16(38), 11549-11553.

Sun, F., Zhang, G., Zhang, D., Xue, L., & Jiang, H. (2011). Aqueous fluorescence turn-on sensor for Zn²⁺ with a tetraphenylethylene compound. *Organic letters*, 13(24), 6378-6381.

Wang, L., Yang, Z., Gao, J., Xu, K., Gu, H., Zhang, B., ... & Xu, B. (2006). A biocompatible method of decorporation: bisphosphonate-modified magnetite nanoparticles to remove uranyl ions from blood. *Journal of the American Chemical Society*, 128(41), 13358-13359.

Wang, Y., Peng, X., Shi, J., Tang, X., Jiang, J., & Liu, W. (2012). Highly selective fluorescent chemosensor for Zn²⁺ derived from inorganic-organic hybrid magnetic core/shell Fe₃O₄@ SiO₂ nanoparticles. *Nanoscale research letters*, 7(1), 1-13.

Wei, H., Insin, N., Lee, J., Han, H. S., Cordero, J. M., Liu, W., & Bawendi, M. G. (2011). Compact zwitterion-coated iron oxide nanoparticles for biological applications. *Nano letters*, 12(1), 22-25.

Xu, Z., Baek, K. H., Kim, H. N., Cui, J., Qian, X., Spring, D. R., ... & Yoon, J. (2009). Zn²⁺-triggered amide tautomerization produces a highly Zn²⁺-selective, cell-permeable, and ratiometric fluorescent sensor. *Journal of the American Chemical Society*, 132(2), 601-610.

Xue, L., Liu, C., & Jiang, H. (2009). Highly sensitive and selective fluorescent sensor for distinguishing cadmium from zinc ions in aqueous media. *Organic letters*, 11(7), 1655-1658.

Xue, L., Li, G., Zhu, D., Liu, Q., & Jiang, H. (2012). Rational design of a ratiometric and targetable fluorescent probe for imaging lysosomal zinc ions. *Inorganic chemistry*, 51(20), 10842-10849.

Yong, R. N., Warkentin, B. P., Phadungchewit, Y., & Galvez, R. (1990). Buffer capacity and lead retention in some clay materials. *Water, Air, and Soil Pollution*, 53(1-2), 53-67.

Zhang, X., Shen, Y., Zhang, H., Jin, J., & Zhou, S. (2015). A new bifunctional fluorescent sensor based on naphthalimide-functionalized silica nanoparticles for detection and adsorption of Cu²⁺ in aqueous solution. *Analytical Methods*, 7(20), 8925-8930.

초 록

일반적인 토양의 중금속 오염도 측정은 전처리 과정을 거친 후 원자흡광분광광도계 또는 유도결합플라즈마-원자발광분광법을 이용해 농도를 분석한다. 이러한 고가의 분석 장비는 휴대가 불가능하여 오염토양의 오염도를 현장에서 측정하기가 어렵다. 따라서 본 연구에서는 고가의 분석장비를 사용하지 않는 형광화학센서를 기반으로 한 현장 오염도 측정 기술을 제시하고자 한다. 본 연구에서 사용된 형광화학센서는 수용기로 dipocolylamine, 형광체로 나프탈이미드를 결합한 화합물 **2**이고, **2**를 자성이 있는 산화철 나노 입자에 결합시킨 화합물 **1**를 이용해 토양 용출용출액에 존재하는 아연 이온을 선택적으로 검출하고자 한다. 화합물 **2**와 **1**을 이용해 선택성을 검증 하였다. **2**와 **1** 모두 아연 이온과 결합해 527nm 에서 형광 강도가 급격하게 증가하는 것을 확인 할 수 있었다. 정량의 가능성을 평가 하기 위해 아연 적정 실험을 수행한 결과, **2** (10 μ M)는 0-7 μ M 아연 이온 농도에 대해 선형적으로 형광강도가 증가하는 것을 확인 할 수 있었다. 또한 **1** (0.33 wt%) 는 0-20 μ M 아연 이온 농도에 대해 선형적으로 형광 강도가 증가하는 것을 확인 할 수 있었다. 특히 화합물 **1**의 검출한계는 0.0345 ppb 로 측정 되었다. 추가적으로 아연 이온의

선택적으로 검출 할 수 있는 배경 용액의 pH 범위를 실험을 통해 구한 결과 2는 pH 3-11 에서 안정적으로 아연 이온을 검출 할 수 있는 것으로 확인되었다. 실제 오염 토양에 존재하는 아연 이온을 검출 한결과 6% 오차 범위 내에서 검출 되었다.

주요어 : 아연, 토양오염, 산화철나노입자, 나프탈이미드

학 번 : 2015-21280